Journal of Petroleum Exploration and Production Technology (2024) 14:125–137
https://doi.org/10.1007/s13202-023-01709-z

ORIGINAL PAPER-EXPLORATION ENGINEERING

Optimal path planning for directional wells across flow units' many-targets

C. P. B. Fernandes[1] · W. P. Coutinho[2] · J. W. L. Silva[1] · M. D. Santos[1] · G. P. Oliveira[1]

Received: 17 April 2023 / Accepted: 26 September 2023 / Published online: 24 October 2023

Abstract

Over the past decades, directional drilling has continuously advanced to increase hydrocarbon recovery by effectively targeting high-productivity reservoirs. However, many existing approaches primarily focus on heuristic optimization algorithms. Moreover, existing models often neglect the incorporation of petrophysical attributes that can significantly impact the selection of production targets, such as the reservoir quality indicator. This article introduces a novel application of mixed-integer programming to define directional drilling paths, considering practical aspects of interest. The paths are subject to drift angle constraints and reference coordinates that align with the optimal reservoir targets. Such targets are identified using the authors' proposed technique of maximum closeness centrality and the geologic model of hydraulic flow units. In order to evaluate the effectiveness of this approach, a realistic model of the Campos Basin in Brazil is studied. The results reveal that the highest recovery factors obtained with the proposed methodology (17%) exceed the historical average recovery factor of the studied reservoir (15.66%). We believe this study can contribute to the ongoing efforts to enhance directional drilling and maximize the production potential of offshore oil and gas reservoirs.

Keywords Exploration and production · Well drilling · Hydraulic flow units · Mixed-integer programming

List of symbols

c	Cells
$C_{D,q}$	Rock cluster domain
c_s	Seed cell
F_s	Grain shape factor
$G_{D,q}$	Graph
k	Permeability
L	Maximum measured depth
L_{ij}	Euclidean norm
MCC	Maximum closeness centrality
$M_{D,q}$	Maximum closeness centrality cell (MaxC)
n_p	Active cells
p_i	"Prize"
S_{Vgr}	Surface area per unit grain volume
T_i	Drilling targets
u_i	Auxiliary variables
v	Node
α	Drift angles
β	Mapping
ϕ	Porosity
γ	Closeness centrality
Ω	Oilfield domain
σ	Density, kg/m^3
τ	Pore tortuosity
μ_{ij}	Decision variables
ν	Oil viscosity unity, centipoise

Abbreviations

ANP	Petroleum National Agency
COP	Cumulative Oil Production

W. P. Coutinho, J. W. L. Silva and M. D. Santos have contributed equally to this work.

✉ C. P. B. Fernandes
borgesclarissa@gmail.com

W. P. Coutinho
walton.coutinho@ufpe.br

J. W. L. Silva
jose.wilker@academico.ufpb.br

M. D. Santos
mdantas@ci.ufpb.br

G. P. Oliveira
gustavo.oliveira@ci.ufpb.br

[1] TRIL Lab, Federal University of Paraíba, João Pessoa, Paraíba, Brazil

[2] Department of Technology, Federal University of Pernambuco, Av. Marielle Franco, s/n, km 59, Caruaru, Pernambuco, Brazil

DDSP	Directional Drilling Steering Problem
DP	Drilling Paths
DRT	Discrete Rock Typing
ERW	Extended-Reach Well
FZI	Flow Zone Indicator
HFUs	Hydraulic Flow Units
MCC	Cell Maximum Closeness Centrality Cell
MCC-HFU	Maximum Closeness Centrality sites in Hydraulic Flow Units
ORF	Oil Recovery Factor
PDTs	Possible Drilling Targets
RQI	Reservoir Quality Index
TVD	True Vertical Depth
UNISIM-I-D	Namorado sandstone oilfield (Campos Basin, Brazil)

Introduction

Directional drilling became part of the oil and gas (O &G) industry in the 1950 s. Revived three to four decades later, bolder and smarter structures were designed as a response to the challenges of reaching reserves at increasing depths, circumventing geologic obstacles, and optimizing engineering costs (Short 1993). Most of the wells drilled worldwide roughly fall into one of the following categories: vertical, horizontal, directional, or multilateral (Fig. 1).

Vertical wells theoretically extend downwards at a 0-degree azimuth angle from the trunk axis. However, this idealized configuration is practically infeasible in reservoirs due to physical factors that slant the well to some extent. Horizontal wells usually hold a long horizontal displacement at a given depth. Directional wells are determined by any intentional deviation of its trajectory by an azimuth angle generally within 20 to 80 degrees from the trunk (Ma et al. 2016). Multilateral wells are structures split into branches that follow independent directions. Since the directionality features a deviation from the well's trunk, directional wells are, in fact, a superclass that abridges all others.

In order to succeed, directional wells require careful trajectory planning, accurate specification of target zones and stations, and geosteering devices. This is usually done by a multidisciplinary team of geologists, reservoir engineers and completion technicians. Well trajectories depart from the wellhead and usually deviate from the kick-off point toward fixed locations. Such trajectories must usually obey curvature constraints in the form of "build," "hold," and "drop"-like segments, cutting the reservoir 3D space into convenient reference frames and coordinate systems. That said, directional drilling's golden goal is to reach targets accurately and safely at the lowest possible cost (Griffiths 2009).

As they cover a larger perforated surface area, they can reach measured depths above 10,000 m even with smaller true vertical depths (Fig. 2) and eventually leverage the oilfield's production volume (Eren and Suicmez 2020). On the other hand, such distinctions may not ensure high expected recovery rates in all reservoirs because of natural hindrances, operational inaccuracies, or even bad screening of sweet spots.

Considering all the Brazilian basins, the global average recovery factor closed, in 2021, around 13.5% (Fig. 3). The Campos Basin, for example, the country's top producer both in oil and gas resources, comprised around 1360 directional wells in 2021, i.e., 39% of all 3524 (1281 vertical + 883 horizontal) wells. Even so, the recovery factor for the basin stagnated close to 15.66%, considered low compared to its oil-in-place volume.

Although there is no dominant justification for this uneven performance, sub-economic and dry wells are certainly two villains that restrain this number to achieve higher plateaus. Looking at this fact, we find indications of the realistic gap found in the O &G industry regarding well placement and production strategies involving directional drilling. In

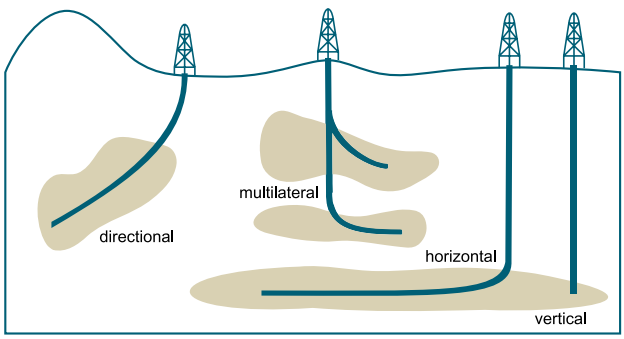

Fig. 1 Usual direction categories of well drilling from azimuth angle variation in relation to the trunk: vertical (permanent 0-degree); horizontal (long near 90-degree displacement); directional (variable 20 to 80-degree deviation); multilateral (variable-angle directional ramifications)

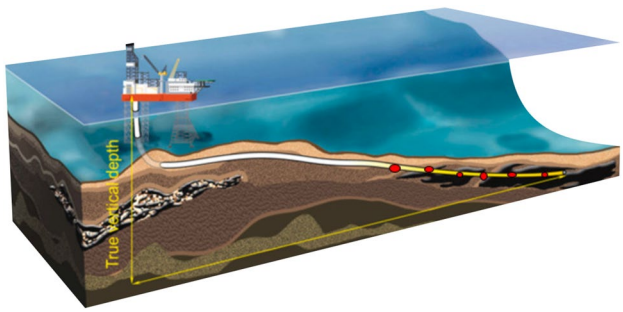

Fig. 2 Sketch of extended-reach well (ERW) drilling. ERWs have a horizontal departure at least twice the true vertical depth (TVD) and a hold-like segment that allows reaching targets with large horizontal displacement from the source. Source: adapted from K. A. Deng's blog (available at https://t.ly/dFMlE)

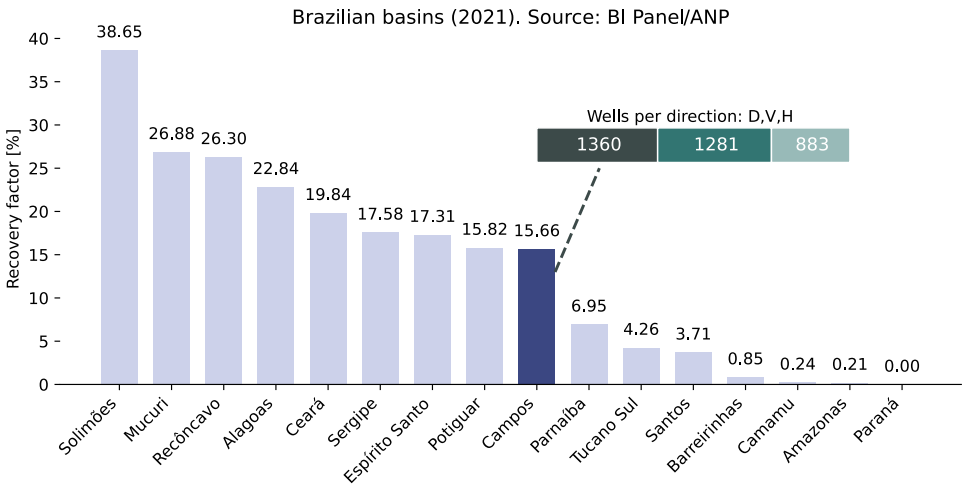

Fig. 3 Global recovery factor of all Brazilian petroleum basins for 2021. Highlight is given to Campos Basin's outcome and its number of wells per direction: directional (D), vertical (V), and horizontal (H)

particular, we identified that integrated approaches combining well placement, sweet spot screening and directional well trajectory optimization are not broadly available, mainly when offshore deep-water environments are under focus.

Of abundant literature, methods and techniques that cope with well trajectory optimization have been largely studied within the theoretical framework. However, most existing approaches give less consideration to petrophysical aspects that can play a determinant role in pre-selecting production targets.

A number of heuristic algorithms have been proposed for computing optimal drilling trajectories from one source point to a single target location. In Atashnezhad et al. (2014), a novel heuristic approach for drilling trajectory design, based on Particle Swarm Optimization (PSO), is proposed to find the optimal measured drilling depth for directional and horizontal wells in a 3D space. A similar approach is employed by Zheng et al. (2019) to solve the established three-objective well trajectory design problem. Huang et al. (2020) developed an algorithm based on the Non-dominated Sorting Genetic Algorithm II (NSGA) in order to solve a multi-objective optimization problem with parameter uncertainties. In Huang et al. (2021), a drilling trajectory design problem is addressed. With the purpose of ensuring safety and increasing efficiency in industrial drilling processes, a new optimization algorithm based on penalty functions and an evolutionary paradigm is developed. An evaluation approach based on fuzzy entropy is further employed to determine a satisfactory solution from the obtained solution set. Finally, in Biswas et al. (2022), a nature-inspired heuristic algorithm is proposed to optimize drilling trajectories so as to reduce the risk of accidents and improve efficiency.

Optimization methods are present in uncountable O &G operations from upstream to downstream (Tavallali et al. 2016; Khor et al. 2017). Regarding the specific problem of determining optimal well trajectories, one observes that constrained curvature based on the Dubins vehicle model predominates. Other theory-centered approaches cover a sequential gradient-restoration algorithm (McCann and Suryanarayana 2001), dynamic systems (Gong et al. 2016), multi-objective optimization (Wang and Gao 2016; Wang et al. 2016), vector-algebra (Wang et al. 2019), improved tangentials (Eren and Suicmez 2020), the Hooke-Jeeves algorithm (Liu et al. 2022), the Dubins model (Liu et al. 2022), and evolutionary search subject to Pareto optimality (D'Angelo et al. 2022). We highlight however that the aforementioned approaches only consider well trajectories between one source location and a single target.

Practice-centered methods seek to minimally embody elements inherent to the reservoir which may affect the correctness of path planning. Rock's resistance to drill bit penetration (Almedallah et al. 2021), obstructing fracturing in tight formations (Gu et al. 2022) and productivity potential maps (Lyu et al. 2021) are included in recent attempts. While it is true that optimization algorithms were not left aside in all these cases, we stress that the addition of subjacent field variables as part of their input data is crucial for determining their targets.

The selection of targets can be seen as a screening task in preparation for assisted drilling. Several heuristic algorithms have been proposed in the literature to tackle this problem. The combination of several PSO algorithms and quality maps is applied for well placement optimization in (Ding et al. 2014). Cellular automata, gray wolf optimization and PSO are integrated by (Biswas et al. 2021) in order to solve a multi-objective problem. Operational constraints such as true vertical depth and casing, along with the bounds of tuning variables, are considered during optimization. In (Yousefzadeh et al. 2021), a method is proposed that combines the fast-marching method and PSO to reduce the number of function evaluations in optimizing the location of vertical injection wells. Sun and Ertekin (2022) present a class of expert systems based on trained and tested artificial neural networks using field data collected from a North American oilfield. These systems are

capable of generating artificial well profiles and evaluating hydrocarbon productivity under hypothetical conditions. In (Yousefzadeh et al. 2022), a workflow based on the so-called reservoir opportunity index maps is employed to optimize the location of production wells under geological uncertainty.

The main argument for this paper is the following: *providing foreknown sweet spots as targets to whatsoever optimization algorithms help to alleviate the algorithmic burden in searching optimal solutions subject to many dynamic constraints, i.e., those stemming from porous media's reaction during real-time drillings, such as dogleg control, sidetracking extension, casing wear, and bit penetration rate.*

The literature is scarce about practice-centered approaches combining screening and optimization to find optimal trajectories for directional wells respecting the medium's petrophysical features. Except for an earlier study that considered a 3D "shoebox" model to find optimal solutions for a single horizontal well (Kharghoria et al. 2003), to the best of our knowledge, there is no parallel case reported for directional drilling in realistic models endowed with multiple targets.

In this paper, we introduce a methodology for directional well drilling that combines target screening from maximum closeness centrality sites in hydraulic flow units (MCC-HFU) (Oliveira et al. 2016), (Roque et al. 2017), (Oliveira et al. 2020b), (Oliveira et al. 2020a) with mixed-integer programming (MIP) to determine optimal trajectories for directional wells. This core idea allows for the implementation of a Directional Drilling Steering Problem (DDSP) mathematical formulation subject to piecewise drift angle constraints.

We tested the DDSP over UNISIM-I (Avansi and Schiozer 2015), a widely known 3D corner-grid point model of the Namorado sandstone oilfield (Campos Basin, Brazil). By running black-oil simulations, the highest production well obtained an index above 17%, which is considered satisfactory. We highlight that this recovery factor exceeds the historical overall factor for the studied reservoir.

We believe that this study significantly contributes to the existing knowledge in the field of well drilling by providing valuable insights for individuals involved in well path planning, well layout modeling and offshore oil and gas exploration. The integration of petrophysical considerations with an optimization model represents a notable advance in directional drilling practices. By incorporating practical aspects into the decision-making process, this methodology offers the potential to optimize well placement and improve hydrocarbon recovery rates.

The remainder of this paper is organized as follows. Section 2 brings the proposed methodological framework. Sections 2.1 and 2.2 provide details about the studied reservoir and HFU identification, respectively. Sections 2.3 and 2.4 present the proposed approaches for reservoir discretization and target screening. In Sect. 2.5, a mixed-integer programming model for directional well path planning is shown. Numerical results from our computational experiments followed by discussion remarks are carried out in 3 Finally, Sect. 4 concludes this paper.

Methodology

The methodological framework encompasses: (i) reservoir setup; (ii) flow unit identification; (iii) target screening; (iv) well path planning; and (v) production analysis (Fig. 4). We will discuss the former four steps below and the last step in Sect. 3

Reservoir setup

UNISIM-I-D is a corner-point grid model for the offshore sandstone *Namorado* formation (Avansi and Schiozer 2015). With about 36600 cells of individual resolution of $100 \times 100 \times 8$ m^3, it is considered a successful benchmark for the Brazilian O &G industry. The porosity ranges from 0 to 30% as can be seen in the color scale of Fig. 5. In addition, the computational model provides the arithmetic mean values of horizontal permeability k_x and vertical permeability k_y from which the absolute directional permeability is obtained $k_x/k_y \approx 1.68$. For all black-oil simulations performed in this paper, we adopted fluid properties equivalent to light oil, namely $\nu = 1.1cp$ for oil viscosity and $\sigma = 29876Kg/m^3$ for density.

The UNISIM-I-D model is a well-known representation of the *Namorado* formation that has been extensively studied in the literature. We refer the interested reader to, e.g., (Avansi and Schiozer 2015; Oliveira et al. 2016; Roque et al. 2017; Oliveira et al. 2020b, a; Sun and Ertekin 2022) for further information about this model.

Hydraulic flow unit identification

Hydraulic Flow Units (HFUs) are regions inside a reservoir with particular attributes. Such features are listed, for instance,

Fig. 4 Diagram of the major methodological steps adopted in this paper. Source: prepared by the authors

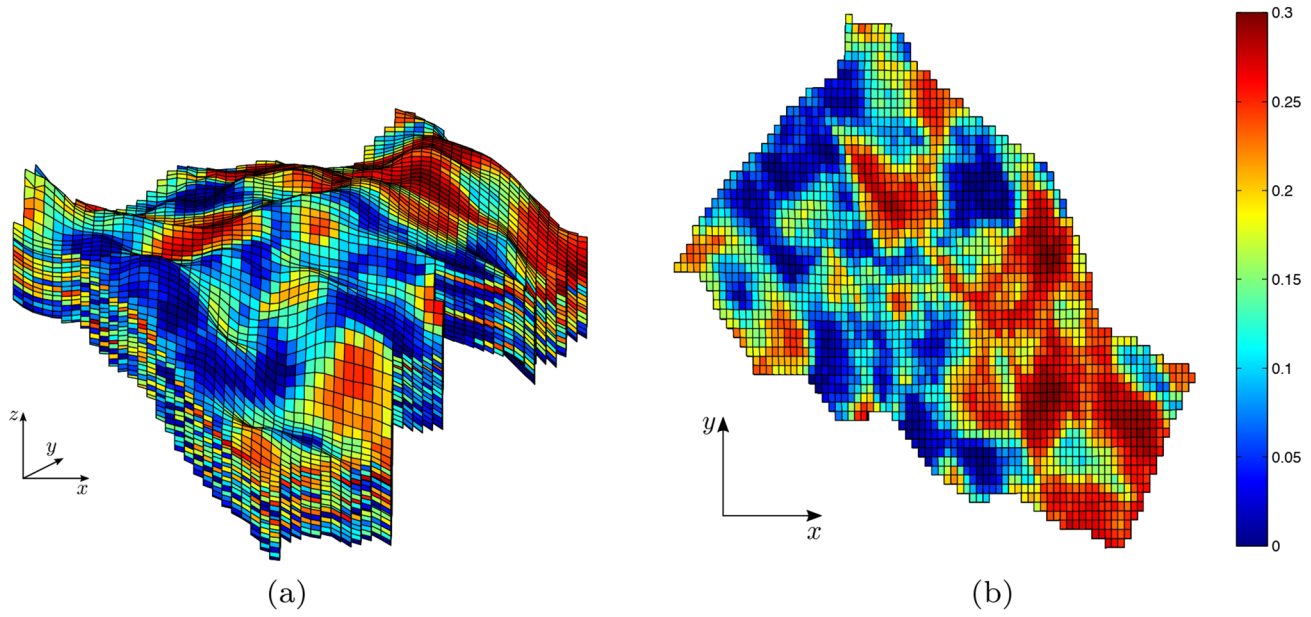

Fig. 5 UNISIM-I-D's porosity field: **a** 3D view and **b** top surface areal view. Source: Roque et al. (2017)

in (Tiab and Donaldson 2015). Tiab and Donaldson (2011) summarize an HFU as being a specific volume of the reservoir, correlative, mappable and recognizable on the wire-line log with the possibility of intercommunication to other HFUs defined in the same way. Among the different definitions of an HFU, we cite Hearn et al. (1984), which says that an HFU is both a laterally and vertically continuous reservoir zone whose permeability, porosity and bedding characteristics are similar.

In a series of earlier papers (Oliveira et al. 2016; Roque et al. 2017; Oliveira et al. 2020b, a), the authors expounded the HFU-maximum closeness centrality (MCC-HFU) approach, its elementary corpus of notation and taxonomy, as well as and how it can be used for well placement strategies. In this paper, we bring a shortened version of the essay to the reader.

HFUs are identified from integrated information of core sampling, wellbore logging, and statistical–petrophysical correlation (Riazi 2018). The current analysis considers Amaefule et al.'s model (AM) to determine HFUs (Amaefule et al. 1993), which rewrites the Kozeny-Carman equation as

$$\mathrm{RQI} \;=\; \mathrm{FZI}\;\phi_z, \tag{1}$$

where ϕ_z is called the pore-to-matrix ratio, RQI is the reservoir quality index, and FZI is the flow zone indicator, respectively, defined as

$$\phi_z = \frac{\phi_e}{1-\phi_e}, \quad \mathrm{RQI} \;= 0.0314\sqrt{\frac{k}{\phi_e}}, \quad \text{and} \quad \mathrm{FZI} \;= \frac{1}{\sqrt{F_s}\tau S_{Vgr}}. \tag{2}$$

A log-log equation is then obtained from Eq. 1 as

$$\log(\,\mathrm{RQI}\,) = \log(\,\mathrm{FZI}\,) + \log(\phi_z), \tag{3}$$

which says that each sample with similar FZI should lie on a straight line of slope equals to 1.0.

The FZI points resulting from this correlation are mapped into a set of discrete cells and used as input to a connected component algorithm that joins cells whose pore throat attributes at the physical domain are similar into "clusters". All these resulting clusters define theoretical flow units, i.e., volumes over which the FZI multimodal distribution varies slightly from a local average (mode).

To convert FZI values from a continuous distribution to a discrete one that associates integer numbers to each rock type detectable over the reservoir model, arbitrary constants a_1 and a_2 fit the following nearest integer function (Guo et al. 2005)

$$\mathrm{DRT} \;= \lfloor a_1 \log(\,\mathrm{FZI}) + a_2 \rceil, \quad a_1, a_2 \in \mathbb{R}, \tag{4}$$

to establish *discrete rock typing*.

The main challenge regarding the MCC-HFU approach is mapping the porosity and permeability fields of a given reservoir into the computational model. This method is less efficient if not enough data is available about a given reservoir. This is not the case for the UNISIM-I-D model though. Therefore, as shown in (Oliveira et al. 2016; Roque et al. 2017; Oliveira et al. 2020b, a), the MCC-HFU method is suitable for a satisfactory representation of the reservoir's physical properties.

Reservoir discretization

Flow units are like a set of neighboring cells on a 3D corner-point grid. Each cell c of the model is addressed by a triplet of logical indices, such that the oilfield domain is defined by the set (Avansi and Schiozer 2015)

$$\overline{\Omega} = \{c_{(i,j,k)}; 1 \leq i \leq I, 1 \leq j \leq J, 1 \leq k \leq K\}, I, J, K \in \mathbb{Z}_{+}^{*}, \tag{5}$$

for a total number of n_p active cells. Here, $\overline{\Omega}$ plays the role of the discrete version of an entire oilfield (major instance). Reservoirs are subsets of $\overline{\Omega}$ (minor instances), all-connected, but with fewer computational cells. Depending on the quantities of interest, the instances can be endowed with finite tuples attributes $(\beta_1, \beta_2, \ldots, \beta_m)$ so that, for example,

$$\beta_a(\overline{\Omega}) = \beta_a(c_{(i,j,k)}) \in \mathbb{R}, \ a = 1, 2, \ldots, m, \ \ \forall i, j, k \tag{6}$$

holds. These attributes are scalar fields like porosity, pressure, and fluid saturations. Likewise, vector or tensor quantities, such as velocity or permeability, are treatable by storing their components individually.

Target screening

In a seminal paper, a few years ago, the authors have proposed a type of pore network model to locate prospective points for well placement in reservoirs (Oliveira et al. 2016). We took advantage of the main steps of such method to guide the screening process for directional drilling. In the end, those prospective points will play the role of drilling targets.

First, the method searches for DRT-based clusters defined by

$$C_{D,q} := \{c \in \overline{\Omega};\ \mathrm{DRT}\,(c) = D \,\mathrm{and}\, c \in N_6(c_s)\}, \quad q = 1, 2, \ldots, Q, \tag{7}$$

where c is an arbitrary cell of the instance $\overline{\Omega}$, N_6 is a 6-neighbor face-connected aggregator which provides the dynamic connectivity among the cells, N_6 a structuring element formed by a seed cell c_s plus its six neighbor cells (in the sense of a Moore's neighborhood) which provides the dynamic connectivity, q is the cluster index and Q is the total amount of distinct clusters generated per DRT value. That is to say, each cluster has a varying number n_q of interconnected cells and form a family of disjoint rock volumes petrophysically similar.

Second, the cluster $C_{D,q}$ associates to a graph $G_{D,q}$ through the one-to-one function

$$\mathcal{F}: C_{D,q} \to G_{D,q}$$
$$c_q^i \mapsto v_q^i.$$

that maps the cluster's cell c_q^i onto the graph's node v_q^i, for $i = 1, 2, \ldots, n_q$, thus establishing a local connectivity among the neighboring cells (Fig. 6). Since $G_{D,q}$ is an undirected graph, its adjacency matrix is symmetric and sparse.

Third, one computes the closeness centrality of each node $v_q \in G_{D,q}$ as

$$\gamma(v_q) = \frac{1}{\sum_{i=1}^{n_\lambda} d(v_q, v_n)}, \ \ \forall v_n \in G_{D,q}, \ v_n \neq v_q, \tag{8}$$

where $d(v_q, v_n)$ is the shortest path distance between v_q and v_n (Newman 2010), so that this metric gives a measure of the influence of HFU's interior to transport fluid masses. As with closeness centrality relates to communication control in network theory (Freeman 1978), we interpreted it as a gauge of potential fluid flow "hubs". For horizontal and directional wells, this concept is relevant because it exploits wells' ability to capture near-field influx, which is superior to vertical configurations given the larger wells' surface coverage area.

Finally, we compute the *maximum closeness centrality cell* (MCC cell) of the cluster $C_{D,q}$ from its most central isomorphic node v_M, thereby setting $\gamma(v_M) = \max\{\gamma(v)\}, v \in \mathcal{G}_{D,q}$ (Fig. 7).

In other words, all v_M nodes correspond to multiple locations of MCC cells over the reservoir model, which, in this paper, are taken as the targets. By denoting a MCC cell location by $M_{D,q}$, we can define the set of possible drilling targets by the family $\{M_{D,q}\}$. In Roque et al. (2017), we called it the maximum closeness network. However, for the algorithmic usage and purposes of this paper, it will be referred to as *possible drilling targets* (PDTs). With natural ordering, we can denote the PDT set to simply

$$T = \{T_1, T_2, \ldots T_n\}, \tag{9}$$

where n is the total number of MCC cells identified. Since n depends both on the number of rock types and clusters per rock type, the ordering is a consequence of the cardinalities

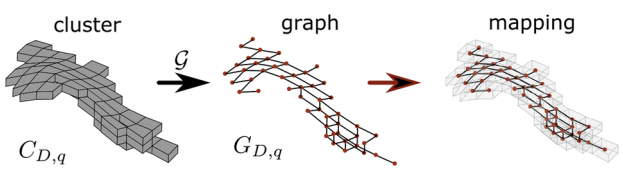

Fig. 6 Geometric interpretation of the cluster-to-graph mapping for a sample volume (flow unit model): $C_{D,q}$ is a cluster formed by face-connected cells of the grid whose cells are mapped onto nodes of the graph $G_{D,q}$. Edges establish the connectivity among the cells. The function $\mathcal{G}$ is one-to-one, so that a the final representation is an isomorphism between cluster and graph. Source: Oliveira et al. (2021)

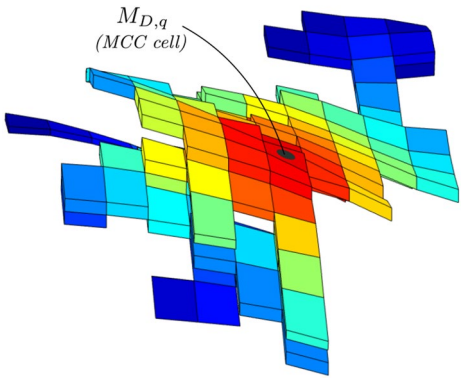

Fig. 7 Example of closeness centrality (γ) distribution over a cluster as a scalar field varying from colder colors (lower γ values) to hotter colors (higher γ values). The central black mark indicates the maximum closeness centrality (MCC) cell denoted by $M_{D,q}$ in harmony with the paper's notation

of both parameters. For instance, for a reservoir model endowed with 3 rock types, let us say $D = \{1, 2, 3\}$, and a cluster distribution per D such as $n_q = \{2, 1, 3\}$, we would have the following correspondences: $T_1 \rightarrow M_{1,1}, T_2 \rightarrow M_{1,2}$, $T_3 \rightarrow M_{2,1}$, $T_4 \rightarrow M_{3,1}$, $T_5 \rightarrow M_{3,2}$, and $T_6 \rightarrow M_{3,3}$, since $n = n_1 + n_2 + n_3 = 2 + 1 + 3 = 6$.

Well path planning

Let us consider: $V = \{1, \ldots, n\}$ the indices of the associated MCC cells T_i (Eq. 9), with 3D spatial coordinates $\mathbf{x}_i = (x_i, y_i, z_i)$ spread over the reservoir (Fig. 8); and $p_i = \log(L_p)$, a cell-weighting parameter, the "prize", $\forall i \in V$, where L_p is the centroid-to-centroid Euclidean distance from a given target cell to its nearest boundary (see Eq. 10d) among all distances L_{cb} from it to each boundary cell (Fig. 9). The values of $p_i, \forall i \in V$, represent yet another measure of the quality of the MCC cells as one seeks to find

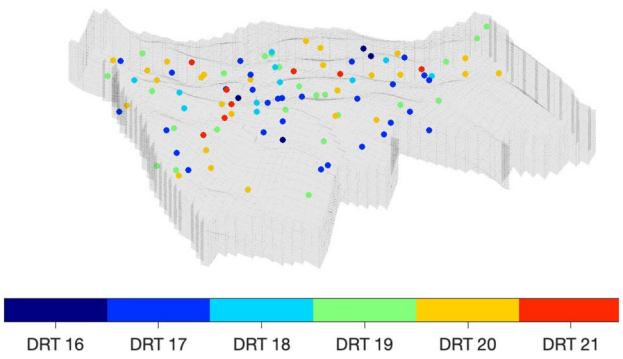

Fig. 8 3D colored scatter plot of all the possible drilling targets (PDTs) categorized by DRT. Depthwise, the PDTs vary along the range 2947.5 – 3192.1 m. As seen in Table 1, there are 101 PDTs

a path over a subset of V that maximizes the potential of petroleum extraction.

For the sake of simplicity, let us also define the set $V' = V \cup \{0\}$, where 0 represents a dummy vertex. The Directional Drilling Steering Problem (DDSP) can be formally stated as follows: find the drilling *path* $r = (i_1, i_2, \ldots, i_q), i \in V, q \leq n$ that maximizes total collected prize $\sum_{i \in r} p_i$ of the visited cells, subject to $\alpha_{ij} \leq \alpha, \forall (i,j) \in s$, and $\sum_{(i,j) \in s} L_{ij} \leq L$, where α is the maximum drift angle between two sequential MCC cells and L is the maximum well's measured depth, given by the sum of all Euclidean distances L_{ij} between each pair T_i, T_j (Fig. 10). We point out that, according to our definition, a *path* describes an ordered subset of drilling targets T_i. This definition should not be misinterpreted as the definition of trajectory, which in this context consists of a function of time describing the well's movement through the oilfield under the action of given forces.

In this paper, the DDSP is modeled as an orienteering problem (Vansteenwegen et al. 2011),(Gunawan et al. 2016), a graph-based approach whose objective is to determine a limited-length route which visits a subset of vertices of a given superset and maximizes the total prize. In fact, the orienteering problem is a variant of the classic Traveling Salesman Problem (Applegate et al. 2006), one of the most famous in the literature of Combinatorial Optimization and Mixed Integer Linear Programming (Jünger 2009). In this paper, all the 101 PDTs play the same role as the salesman's customers (Table 1).

The DDSP's decision variables are: μ_{ij} (binary), which is valued 1 if the path reaches the MCC cells T_i and T_j, subsequently, and 0 otherwise; and $u_i \in \mathbb{Z}^+$, for $i \in V'$, which plays the auxiliary role in representing the cell-visiting order

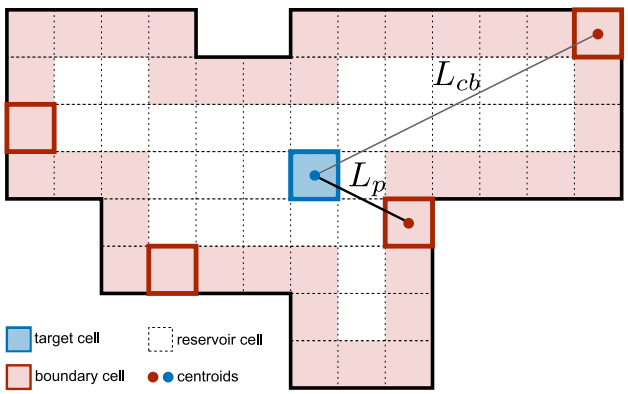

Fig. 9 Scheme that explains the "prize" (p_i) computed over the 3D space. Discrete active cells form the reservoir model from inner cells and boundary cells (shaded stripe). The prize per target cell (shaded in blue) is determined by computing all centroid-to-centroid Euclidean distances (L_{cb}) to the boundary and taking the logarithm of the shortest distance to the boundary, L_p

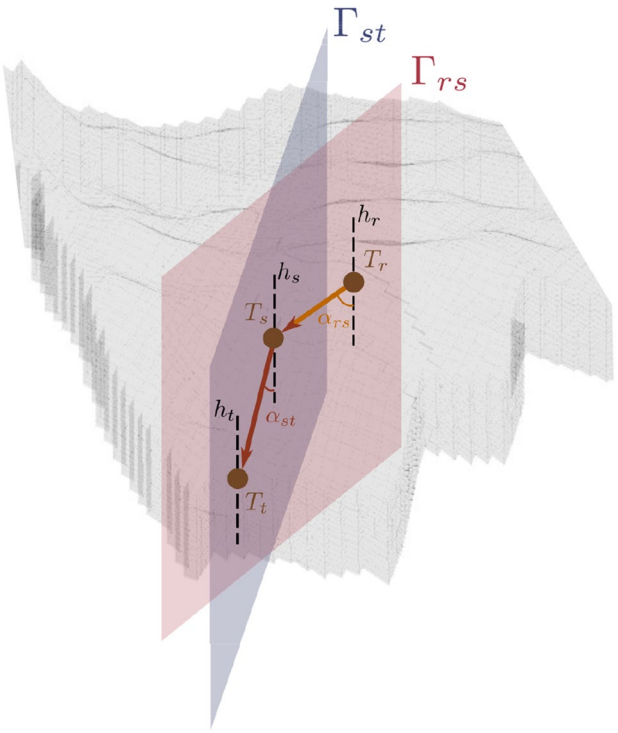

Fig. 10 Scheme of the MILP algorithm applied to reservoir's 3 targets, namely T_r, T_s, and T_t. The plane Γ_{rs} (Γ_{st}) cuts the targets subscripted by r and s (s and t) in parallel to the vertical axes h_r and h_s (h_s and h_t). In the figure, the path starts at T_r, moves to T_s, then to T_t obeying the drift angle constraint $\alpha_{rs}(\alpha_{st}) \leq \alpha$, where α is the maximum drift angle allowable by the user. In this paper, we tested path plannings for $\alpha = \{30, 40, 50, 60, 70, 80\}$

and avoiding *subcycles* (Miller et al. 1960). For the sake of clarity, we expand on the meaning of the decision variables with the following example. Let $r = (0, 2, 4, 1, 3)$ be an optimal drilling path from an arbitrary set of MCC cells (or PDTs). The values of the μ variables associated with this path are $\mu_{02} = \mu_{24} = \mu_{41} = \mu_{13} = 1$, while the remaining μ variables are set to 0. This means that the MCC cells T_0, T_2, T_4, T_1, T_3 are visited in this specific order. In turn, variables u are auxiliary variables used for subcycle elimination. For more information, we refer the interested reader to any literature on vehicle routing problems (Applegate et al. 2006; Vansteenwegen et al. 2011; Toth and Vigo 2014; Gunawan et al. 2016). Since

$$\mu_{ij} \in \{0, 1\} \quad \text{(decision variables)} \tag{10a}$$

$$u_i \in \mathbb{Z}^+ \quad \text{(auxiliary variables)} \tag{10b}$$

$$p_i = \log(L_p) \quad \text{(constant prize)} \tag{10c}$$

$$L_{ij} = || \mathbf{x}_i - \mathbf{x}_j ||_2 \quad \text{(Euclidean norm)} \tag{10d}$$

$$L = 10,000\,[m] \quad \text{(max. measured depth)}, \tag{10e}$$

the DDSP is formally posed as:

$$\max \sum_{i \in V} \sum_{\substack{j \in V' \\ j \neq i}} p_i \mu_{ij} \tag{11a}$$

$$\sum_{j \in V} \mu_{0j} = \sum_{i \in V} \mu_{i0} = 1 \tag{11b}$$

$$\sum_{\substack{i \in V' \\ i \neq j}} \mu_{ij} \leq 1, \forall j \in V \tag{11c}$$

$$\sum_{\substack{j \in V' \\ j \neq i}} \mu_{ij} \leq 1, \forall i \in V \tag{11d}$$

$$\sum_{\substack{i \in V' \\ i \neq k}} \mu_{ik} - \sum_{\substack{j \in V' \\ j \neq k}} \mu_{kj} = 0, \forall k \in V \tag{11e}$$

$$u_j \leq u_i + 1 - n(1 - \mu_{ij}), \forall i, j \in V \tag{11f}$$

$$2 \leq u_i \leq |V'|, \forall i \in V \tag{11g}$$

$$\sum_{i \in V} \sum_{\substack{j \in V \\ j \neq i}} L_{ij} \mu_{ij} \leq L \tag{11h}$$

with $u_0 = 1$. The objective function (11a) maximizes the total collected prize of the visited cells. The constraints to which the objective function are subject encompass single interception, path continuity, the path's maximum measured depth and avoiding solutions having subcycles (Miller et al. 1960). Further detail is available in any literature on routing problems, e.g., (Toth and Vigo 2014). One can observe that formulation (11a)–(11h) is valid for any set of general parameters V, L and α, and cell-dependent parameters p_i and L_{ij}, i and $j \in V$. We do not consider uncertainties regarding these parameters as it would require different optimization techniques (e.g., robust (Ben-Tal et al. 2009) or stochastic optimization (Schneider and Kirkpatrick 2007)) which are considered out of the scope of this paper. In our approach, the appropriate choice of such parameters is left to the technical team working in the field.

Table 1 Set of all possible drilling targets (PSTs) and their associations with maximum closeness centrality point organized by DRT

DRT 16	DRT 17	DRT 18	DRT 19	DRT 20	DRT 21
$M_{16,8} \rightarrow T_1$	$M_{17,1} \rightarrow T_5$	$M_{18,10} \rightarrow T_{34}$	$M_{19,11} \rightarrow T_{45}$	$M_{20,1} \rightarrow T_{68}$	$M_{21,12} \rightarrow T_{94}$
$M_{16,9} \rightarrow T_2$	$M_{17,11} \rightarrow T_6$	$M_{18,17} \rightarrow T_{35}$	$M_{19,12} \rightarrow T_{46}$	$M_{20,11} \rightarrow T_{69}$	$M_{21,15} \rightarrow T_{95}$
$M_{16,12} \rightarrow T_3$	$M_{17,14} \rightarrow T_7$	$M_{18,26} \rightarrow T_{36}$	$M_{19,13} \rightarrow T_{47}$	$M_{20,14} \rightarrow T_{70}$	$M_{21,26} \rightarrow T_{96}$
$M_{16,17} \rightarrow T_4$	$M_{17,22} \rightarrow T_8$	$M_{18,29} \rightarrow T_{37}$	$M_{19,17} \rightarrow T_{48}$	$M_{20,19} \rightarrow T_{71}$	$M_{21,3} \rightarrow T_{97}$
	$M_{17,23} \rightarrow T_9$	$M_{18,37} \rightarrow T_{38}$	$M_{19,19} \rightarrow T_{49}$	$M_{20,2} \rightarrow T_{72}$	$M_{21,38} \rightarrow T_{98}$
	$M_{17,28} \rightarrow T_{10}$	$M_{18,39} \rightarrow T_{39}$	$M_{19,20} \rightarrow T_{50}$	$M_{20,20} \rightarrow T_{73}$	$M_{21,45} \rightarrow T_{99}$
	$M_{17,29} \rightarrow T_{11}$	$M_{18,44} \rightarrow T_{40}$	$M_{19,29} \rightarrow T_{51}$	$M_{20,22} \rightarrow T_{74}$	$M_{21,5} \rightarrow T_{100}$
	$M_{17,30} \rightarrow T_{12}$	$M_{18,49} \rightarrow T_{41}$	$M_{19,32} \rightarrow T_{52}$	$M_{20,27} \rightarrow T_{75}$	$M_{21,8} \rightarrow T_{101}$
	$M_{17,31} \rightarrow T_{13}$	$M_{18,54} \rightarrow T_{42}$	$M_{19,35} \rightarrow T_{53}$	$M_{20,29} \rightarrow T_{76}$	
	$M_{17,35} \rightarrow T_{14}$	$M_{18,59} \rightarrow T_{43}$	$M_{19,36} \rightarrow T_{54}$	$M_{20,30} \rightarrow T_{77}$	
	$M_{17,36} \rightarrow T_{15}$	$M_{18,6} \rightarrow T_{44}$	$M_{19,4} \rightarrow T_{55}$	$M_{20,33} \rightarrow T_{78}$	
	$M_{17,38} \rightarrow T_{16}$		$M_{19,48} \rightarrow T_{56}$	$M_{20,37} \rightarrow T_{79}$	
	$M_{17,4} \rightarrow T_{17}$		$M_{19,49} \rightarrow T_{57}$	$M_{20,38} \rightarrow T_{80}$	
	$M_{17,44} \rightarrow T_{18}$		$M_{19,51} \rightarrow T_{58}$	$M_{20,4} \rightarrow T_{81}$	
	$M_{17,46} \rightarrow T_{19}$		$M_{19,58} \rightarrow T_{59}$	$M_{20,43} \rightarrow T_{82}$	
	$M_{17,51} \rightarrow T_{20}$		$M_{19,59} \rightarrow T_{60}$	$M_{20,46} \rightarrow T_{83}$	
	$M_{17,52} \rightarrow T_{21}$		$M_{19,63} \rightarrow T_{61}$	$M_{20,48} \rightarrow T_{84}$	
	$M_{17,6} \rightarrow T_{22}$		$M_{19,67} \rightarrow T_{62}$	$M_{20,50} \rightarrow T_{85}$	
	$M_{17,62} \rightarrow T_{23}$		$M_{19,70} \rightarrow T_{63}$	$M_{20,52} \rightarrow T_{86}$	
	$M_{17,63} \rightarrow T_{24}$		$M_{19,77} \rightarrow T_{64}$	$M_{20,57} \rightarrow T_{87}$	
	$M_{17,64} \rightarrow T_{25}$		$M_{19,8} \rightarrow T_{65}$	$M_{20,64} \rightarrow T_{88}$	
	$M_{17,65} \rightarrow T_{26}$		$M_{19,82} \rightarrow T_{66}$	$M_{20,65} \rightarrow T_{89}$	
	$M_{17,7} \rightarrow T_{27}$		$M_{19,83} \rightarrow T_{67}$	$M_{20,67} \rightarrow T_{90}$	
	$M_{17,75} \rightarrow T_{28}$			$M_{20,72} \rightarrow T_{91}$	
	$M_{17,77} \rightarrow T_{29}$			$M_{20,73} \rightarrow T_{92}$	
	$m_{17,78} \rightarrow T_{30}$			$M_{20,9} \rightarrow T_{93}$	
	$M_{17,9} \rightarrow T_{31}$				
	$m_{17,92} \rightarrow T_{32}$				
	$M_{17,95} \rightarrow T_{33}$				

Results and discussion

Directional paths

From formulation (11a–11h), we generated 6 distinct drilling paths (DP) subject to drift angles $\alpha = \{30, 40, 50, 60, 70, 80\}$ (Table 2). One verifies that they cross 12, 13, 15, 16, 17, and 18 flow unit targets, respectively. The increasing number of targets is a consequence of the drift angle relaxation, which allows for enlarged coverage of the geologic units.

The DDSP formulation was coded using the `Pyomo` (v. 6.4.4) modeling language through its `Python` interface (v. 3.8) and solved by the software `CPLEX` (v. 12.7) in an Intel i7 CPU with 3.60GHz and 24GB of RAM running under Linux Mint 20.2 64bits. The 6 generated DPs were computed in about 1 s on average, showing that the proposed approach scales well in practice. The TSP literature shows that larger and more complex case studies can be efficiently solved with minor modifications to the proposed formulation Applegate et al. (2006); Toth and Vigo (2014) (Figs. 11, 12 and 13).

Production analysis

In order to analyze the technical and economic feasibility of the proposed methodology, we carried out tests of cumulative oil production (COP) and oil recovery factor (ORF). The ORF measures how much of the oil-in-place can be extracted using the available technology over a time period. Both COP and ORF metrics are commonly used by the scientific literature and industry (Hersir et al. 2022). Fig. 14 is a plot of COP curves for all paths. In all cases, the wells reached high oil production, as they are strategically intercepting oil-saturated HFUs. One observes that the highest production was obtained for DP70 and the lowest one for DP40.

Our experiments indicate that there is no direct relationship between the number of visited HFUs and metrics such as COP and ORF. Meaning that shorter paths visiting a smaller number of HFUs might present better oil

Table 2 Optimum solutions for directional paths generated from the MILP algorithm

ID	α	$M_{D,q}$	T
DP30	30	$M_{19,36}$,$M_{20,22}$,$M_{17,23}$,$M_{17,78}$,$M_{20,27}$, $M_{18,17}$,$M_{21,5}$,$M_{19,17}$,$M_{20,9}$,$M_{17,31}$, $M_{16,12}$,$M_{17,44}$	T_{54},T_{74},T_{9},T_{30},T_{75}, T_{35},T_{100}, T_{48},T_{93}, T_{13}, T_{3},T_{18}
DP40	40	$M_{20,27}$,$M_{18,17}$,$M_{21,5}$,$M_{19,17}$,$M_{17,35}$, $M_{20,20}$,$M_{20,38}$,$M_{17,36}$,$M_{17,77}$,$M_{16,12}$, $M_{17,38}$,$M_{20,37}$,$M_{19,19}$	T_{75},T_{35},T_{100},T_{48},T_{14}, T_{73},T_{80},T_{15}, T_{29},T_{3}, T_{16},T_{79},T_{49}
DP50	50	$M_{20,22}$,$M_{17,23}$,$M_{20,27}$,$M_{17,1}$,$M_{20,67}$, $M_{19,17}$,$M_{17,35}$,$M_{20,20}$,$M_{20,38}$,$M_{17,31}$, $M_{16,12}$,$M_{17,38}$,$M_{17,29}$,$M_{20,37}$,$M_{19,19}$	T_{74},T_{9},T_{75},T_{5},T_{90}, T_{48},T_{14}, T_{73},T_{80}, T_{13}, T_{3},T_{16},T_{11},T_{79},T_{49}
DP60	60	$M_{20,22}$,$M_{17,23}$,$M_{20,27}$,$M_{17,1}$,$M_{17,11}$, $M_{18,17}$,$M_{21,5}$,$M_{17,92}$,$M_{20,67}$,$M_{19,17}$, $M_{21,26}$,$M_{17,75}$,$M_{17,46}$,$M_{17,29}$,$M_{20,37}$, $M_{19,19}$	T_{74},T_{9},T_{75},T_{5},T_{6}, T_{35},T_{100}, T_{32},T_{90}, T_{48},T_{96},T_{28},T_{19},T_{11}, T_{79},T_{49}
DP70	70	$M_{20,22}$,$M_{17,23}$,$M_{20,27}$,$M_{17,1}$,$M_{17,11}$, $M_{18,17}$,$M_{21,5}$,$M_{19,17}$,$M_{20,9}$,$M_{21,26}$, $M_{17,31}$,$M_{16,12}$,$M_{17,46}$,$M_{17,29}$,$M_{20,37}$, $M_{19,63}$,$M_{20,48}$	T_{74},T_{9},T_{75},T_{5},T_{6}, T_{35},T_{100}, T_{48},T_{93}, T_{96}, T_{13},T_{3},T_{19},T_{11},T_{79}, T_{61},T_{84}
DP80	80	$M_{20,22}$,$M_{17,23}$,$M_{20,27}$,$M_{17,1}$,$M_{17,11}$, $M_{18,17}$,$M_{21,5}$,$M_{17,92}$,$M_{19,17}$,$M_{17,7}$, $M_{17,31}$,$M_{16,12}$,$M_{19,4}$,$M_{17,46}$,$M_{17,29}$, $M_{20,37}$,$M_{19,63}$,$M_{20,48}$	T_{74},T_{9},T_{75},T_{5},T_{6}, T_{35},T_{100}, T_{32},T_{48}, T_{27}, T_{13},T_{3},T_{55},T_{19},T_{11}, T_{79},T_{61},T_{84}

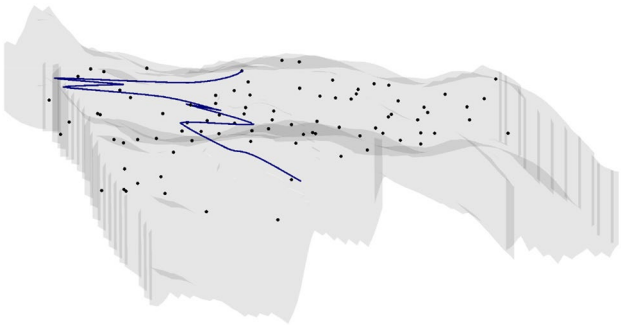

Fig. 11 3D view of selected well trajectories generated by the MILP algorithm for DP30. The paths cross flow unit targets among all possible drilling targets (black points). For the sake of visualization, the generated paths have been smoothly interpolated through the application of 3D splines over the generated paths

production than longer paths visiting a different set of HFUs (Figures 3.2 and 3.2). For example, solution DP30 shows better performance than DP40, DP50 and DP60 in all experiments. However, a careful analysis of the generated drilling paths indicates that higher production metrics are achieved by paths that intercept target points with better flow capacity.

HFUs primarily indicate regions with the highest flow capacity, regardless of the specific fluid type. In the case of HFUs located in completely oil-saturated regions, production is expected to be significantly higher. Since the target points (18 points) of path DP70 intersect regions with high oil saturation, higher oil production is consequently

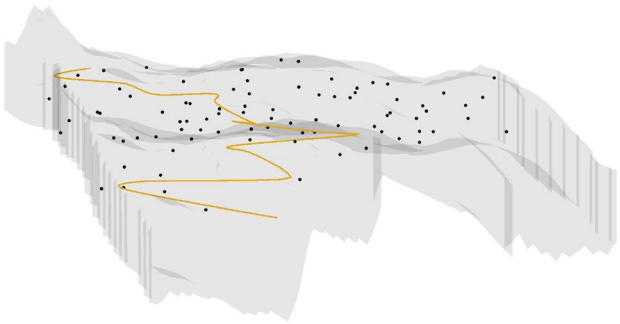

Fig. 12 3D view of selected well trajectories generated by the MILP algorithm for DP50. The paths cross flow unit targets among all possible drilling targets (black points). For the sake of visualization, the generated paths have been smoothly interpolated through the application of 3D splines over the generated paths

Fig. 13 3D view of selected well trajectories generated by the MILP algorithm for DP70. The paths cross flow unit targets among all possible drilling targets (black points). For the sake of visualization, the generated paths have been smoothly interpolated through the application of 3D splines over the generated paths

achieved. Compared to the DP70, DP40 intercepts a smaller number of high saturated target points (13 points), which results in lower oil production metrics (Figures 3.2 and 3.2).

Also, we identified that the lowest ORF is given by DP40, with ORF greater than 10%, whereas the highest one is associated with DP70, reaching about 17%, which is a value higher than the Campos Basin's ORF, which reached approximately 15.6% (Fig. 3). Therefore, from these numbers, we can observe that the methodology used here increases the ORF by about 8%.

Conclusions

- This research paper focuses on the development of directional well paths using a variant of the Traveling Salesman problem.

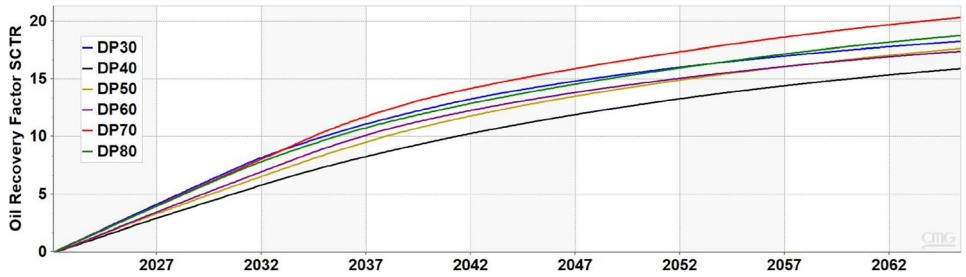

(a) Oil recovery factor - ORF

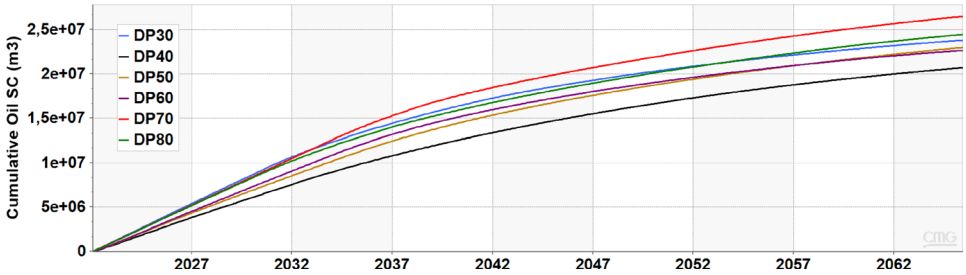

(b) Cumulative oil production - COP.

Fig. 14 Production curves for all drilling paths simulated from CMG Imex software

- The objective was to establish optimal drilling paths that pass through multiple potential targets, identified based on flow units.
- The optimization process considered drift angle constraints ranging from 30 to 80 degrees and a measured depth limit of 10,000 ms. As a case study, a synthetic model was created to resemble the characteristics of the Namorado oilfield.
- The performance of the optimized well paths was evaluated using oil recovery factor and cumulative oil production as metrics. These metrics were compared with data from the Brazilian Campos Basin to validate the results.
- The results of the study demonstrated that the well with the highest production achieved a recovery factor index above 17%, which is considered satisfactory. This result outperforms the average recovery factor of Brazilian basins, which stood at around 13.5% in 2021. Moreover, it exceeds the recovery factor of the Campos Basin, which was reported to be 16.5%. These findings highlight the effectiveness of the proposed methodology in enhancing oil recovery.
- Future research directions involve the integration of additional factors into the framework. This includes incorporating productivity potential maps, generating well trajectories considering in situ geologic constraints, exploring the feasibility of multilateral wells, and conducting economic analysis. These enhancements aim to further optimize well planning and maximize hydrocarbon production in complex reservoirs.

Funding Partial financial support was received from FAPESQ-PB, Brazil.

Declarations

Conflict of interest The authors have no competing interests to declare that are relevant to the content of this article.

References

Almedallah M, Al Mudhafar A, Clark S, Walsh S (2021) Vector-based threedimensional (3d) well-path optimization assisted by geological modelling and borehole-log extraction. Upstream Oil Gas Technol. https://doi.org/10.1016/j.upstre.2021.100053

Amaefule JO, Altunbay M, Tiab D, Kersey DG, Keelan DK (1993). Enhanced reservoir description: using core and log data to identify hydraulic (flow) units and predict permeability in uncored intervals/wells. Spe annual technical conference and exhibition (p. SPE-26436-MS)

Applegate DL, Bixby RE, Chvatál V, Cook WJ (2006). The traveling salesman problem: A computational study. Princeton University

Press. Retrieved 2022-10-27, from http://www.jstor.org/stable/j.ctt7s8xg
Atashnezhad A, Wood DA, Fereidounpour A, Khosravanian R (2014) Designing and optimizing deviated wellbore trajectories using novel particle swarm algorithms. J Nat Gas Sci Eng 21:1184–1204
Avansi GD, Schiozer DJ (2015) Unisim-i: synthetic model for reservoir development and management applications. Int J Model Simul Petroleum Ind 9(1):21–30
Ben-Tal A, El Ghaoui L, Nemirovski A (2009) Robust optimization, vol 28. Princeton University Press, Princeton
Biswas K, Rahman MT, Almulihi AH, Alassery F, Al Askary MAH, Hai TB, Ahmed R (2022) Uncertainty handling in wellbore trajectory design: a modified cellular spotted hyena optimizer-based approach. J Petroleum xploration Product Technol 12(10):2643–2661
Biswas K, Vasant PM, Vintaned JAG, Watada J (2021) Cellular automata-based multi-objective hybrid grey wolf optimization and particle swarm optimization algorithm for wellbore trajectory optimization. J Nat Gas Sci Eng 85:103695
D'Angelo J, Khaled M, Ashok P, van Oort E (2022) Pareto optimal directional drilling advisory for improved real-time decision making. J Petroleum Sci Eng. https://doi.org/10.1016/j.petrol.2021.110031
Ding S, Jiang H, Li J, Tang G (2014) Optimization of well placement by combination of a modified particle swarm optimization algorithm and quality map method. Comput Geosci 18:747–762
Eren T, Suicmez V (2020) Directional drilling positioning calculations. J Nat Gas Sci Eng. https://doi.org/10.1016/j.jngse.2019.103081
Freeman L (1978) Centrality in social networks conceptual clarification. Soc Netw 1(3):215–239
Gong Z, Loxton R, Yu C, Teo K (2016) Dynamic optimization for robust path planning of horizontal oil wells. Appl Math Comput 274:711–725. https://doi.org/10.1016/j.amc.2015.11.038
Griffiths R (2009) Well placement fundamentals. Schlumberger, Boston
Gu Y, Gao D, Diao B, Yang J, Nie S (2022) Optimization design method of infill well trajectory with bypassing obstacles in the fractured area of shale gas reservoir. J Petroleum Sci Eng. https://doi.org/10.1016/j.petrol.2021.109779
Gunawan A, Lau HC, Vansteenwegen P (2016) Orienteering problem: a survey of recent variants, solution approaches and applications. Eur J Oper Res 255(2):315–332. https://doi.org/10.1016/j.ejor.2016.04.059
Guo G et al. (2005). Rock typing as an effective tool for permeability and watersaturation modeling: a case study in a clastic reservoir in the oriente basin. Spe annual technical conference and exhibition (p. SPE 97033- PA)
Hearn C, Ebanks W Jr, Tye R, Ranganathan V (1984) Geological factors influencing reservoir performance of the hartzog draw field, wyoming. J Petrol Technol 36(08):1335–1344
Hersir G, Guðnason EA, Flóvenz OG (2022). 7.04 - geophysical exploration techniques. T.M. Letcher (Ed.), Comprehensive renewable energy (second edition) (Second Edition ed., p. 26-79). Oxford: Elsevier
Huang W, Wu M, Chen L, Chen X, Cao W (2021) Multi-objective drilling trajectory optimization using decomposition method with minimum fuzzy entropybased comprehensive evaluation. Appl Soft Comput 107:107392
Huang W, Wu M, Chen L, She J, Hashimoto H, Kawata S (2020) Multiobjective drilling trajectory optimization considering parameter uncertainties. IEEE Trans Syst, Man, and Cybernetics: Syst 52(2):1224–1233
Jünger M et al. (Eds.). (2009). 50 years of integer programming 1958-2008: From the early years to the state-of-the-art
Kharghoria A, Cakici M, Narayanasamy R, Kalita R, Sinha S, Jalali Y (2003). Productivity-based method for selection of reservoir drilling target and steering strategy. Spe/iadc middle east drilling technology conference and exhibition (pp.SPE-85341)
Khor C, Elkamel A, Shah N (2017) Optimization methods for petroleum fields development and production systems: a review. Optim Eng 18:907–941
Liu H, Gjersvik T, Faanes A (2022) Subsea field layout optimization (part i)- directional well trajectory planning based on 3d dubins curve. J Petroleum Sci Eng. https://doi.org/10.1016/j.petrol.2021.109450
Liu S-J, Zhou X-M, Zhang J-W, Xie Z-D (2022) The optimization algorithm for application in directional drilling trajectories of energy field. Energy Rep 8:1212–1217. https://doi.org/10.1016/j.egyr.2022.01.235
Lyu Z, Lei Q, Yang L, Heaney C, Song X, Salinas P, Pain C (2021) A novel approach to optimising well trajectory in heterogeneous reservoirs based on the fast-marching method. J Nat Gas Sci Eng. https://doi.org/10.1016/j.jngse.2021.103853
Ma T, Chen P, Zhao J (2016) Overview on vertical and directional drilling technologies for the exploration and exploitation of deep petroleum resources. Geomech Geophys Geo-Energy Geo-Resour 2(4):365–395. https://doi.org/10.1007/s40948-016-0038-y
McCann R, Suryanarayana P (2001) Horizontal well path planning and correction using optimization techniques. J Energy Resour Technol, Trans ASME 123(3):187–193. https://doi.org/10.1115/1.1386390
Miller CE, Tucker AW, Zemlin RA (1960) Integer programming formulation of traveling salesman problems. J ACM (JACM) 7(4):326–329
Newman M (2010) Networks: An introduction. Oxford University Press, New York
Oliveira G, Araújo E, Santos M, Roque W (2020) Non-uniform injector/producer well pattern designs induced by morphology and anisotropy of flow units. J Petroleum Sci Eng. https://doi.org/10.1016/j.petrol.2019.106680
Oliveira G, Roque W, Araújo E, Diniz A, Simões T, Santos M (2016) Competitive placement of oil perforation zones in hydraulic flow units from centralitymeasures. J Petrol Sci Eng 147:282–291. https://doi.org/10.1016/j.petrol.2016.06.008
Oliveira G, Santos M, Roemers-Oliveira E (2021) Well placement subclustering within partially oil-saturated flow units. J Petroleum Sci Eng. https://doi.org/10.1016/j.petrol.2020.107730
Oliveira G, Santos M, Roque W (2020) Constrained clustering approaches to identify hydraulic flow units in petroleum reservoirs. J Petroleum Sci Eng. https://doi.org/10.1016/j.petrol.2019.106732
Riazi Z (2018) Application of integrated rock typing and flow units identification methods for an Iranian carbonate reservoir. J Petrol Sci Eng 160:483–497. https://doi.org/10.1016/j.petrol.2017.10.025
Roque W, Oliveira G, Santos M, Simões T (2017) Production zone placements based on maximum closeness centrality as strategy for oil recovery. J Petrol Sci Eng 156:430–441. https://doi.org/10.1016/j.petrol.2017.06.016
Schneider J, Kirkpatrick S (2007) Stochastic optimization. Springer Science & Business Media, Berlin
Short JA (1993) Introduction to directional and horizontal drilling. Pennwell Corporation, Tulsa
Sun Q, Ertekin T (2022) Structure of an artificial-intelligence-assisted reservoir characterization and field development protocol. Fuel 324:124762
Tavallali M, Karimi I, Baxendale D (2016) Process systems engineering perspective on the planning and development of oil fields. AIChE J 62(8):2586–2604. https://doi.org/10.1002/aic.15209

Tiab D, Donaldson E (2011). Petrophysics: Theory and practice of measuring reservoir rock and fluid transport properties: Elsevier science

Tiab D, Donaldson EC (2015) Petrophysics: theory and practice of measuring reservoir rock and fluid transport properties. Gulf professional publishing, Waltham

Toth P, Vigo D (2014) Vehicle routing: problems, methods, and applications. Society for Industrial and Applied Mathematics, Philadelphia

Vansteenwegen P, Souffriau W, Oudheusden DV (2011) The orienteering problem: a survey. Eur J Oper Res 209(1):1–10. https://doi.org/10.1016/j.ejor.2010.03.045

Wang Z, Gao D (2016) Multi-objective optimization design and control of deviation-correction trajectory with undetermined target. J Nat Gas Sci Eng 33:305–314. https://doi.org/10.1016/j.jngse.2016.05.028

Wang Z, Gao D, Liu J (2016) Multi-objective sidetracking horizontal well trajectory optimization in cluster wells based on ds algorithm. J Petrol Sci Eng 147:771–778. https://doi.org/10.1016/j.petrol.2016.09.046

Wang Z, Gao D, Yang J (2019) Design and calculation of complex directional-well trajectories on the basis of the minimum-curvature method. SPE Drill Complet 43(2):173–188. https://doi.org/10.2118/194511-PA

Yousefzadeh R, Ahmadi M, Kazemi A (2022) Toward investigating the application of reservoir opportunity index in facilitating well placement optimization under geological uncertainty. J Petrol Sci Eng 215:110709

Yousefzadeh R, Sharifi M, Rafiei Y (2021) An efficient method for injection well location optimization using fast marching method. J Petrol Sci Eng 204:108620

Zheng J, Lu C, Gao L (2019) Multi-objective cellular particle swarm optimization for wellbore trajectory design. Appl Soft Comput 77:106–117